ACS OMEGA

http://pubs.acs.org/journal/acsodf

Article

Antiviral Polymer Brushes by Visible-Light-Induced, Oxygen-Tolerant Covalent Surface Coating

Andriy R. Kuzmyn, Lucas W. Teunissen, Michiel V. Kroese, Jet Kant, Sandra Venema, and Han Zuilhof*

Cite This: *ACS Omega* 2022, 7, 38371−38379

Read Online

ACCESS | Metrics & More | Article Recommendations | Supporting Information

ABSTRACT: This work presents a novel route for creating metal-free antiviral coatings based on polymer brushes synthesized by surface-initiated photoinduced electron transfer-reversible addition−fragmentation chain transfer (SI-PET-RAFT) polymerization, applying eosin Y as a photocatalyst, water as a solvent, and visible light as a driving force. The polymer brushes were synthesized using *N*-[3-(decyldimethyl)-aminopropyl] methacrylamide bromide and carboxybetaine methacrylamide monomers. The chemical composition, thickness, roughness, and wettability of the resulting polymer brush coatings were characterized by X-ray photoelectron spectroscopy (XPS), atomic force microscopy (AFM), water contact angle measurements, and ellipsometry. The antiviral properties of coatings were investigated by exposure to severe acute respiratory syndrome coronavirus 2 (SARS-CoV-2) and avian influenza viruses, with further measurement of residual viable viral particles. The best performance was obtained with Cu surfaces, with a ca. 20-fold reduction of SARS-Cov-2 and a 50-fold reduction in avian influenza. On the polymer brush-modified surfaces, the number of viable virus particles decreased by about 5−6 times faster for avian flu and about 2−3 times faster for SARS-CoV-2, all compared to unmodified silicon surfaces. Interestingly, no significant differences were obtained between quaternary ammonium brushes and zwitterionic brushes.

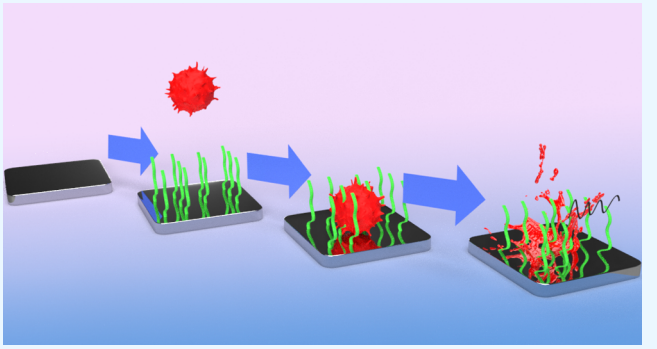

INTRODUCTION

Viruses and virus-related diseases are one of the main reasons for human mortality. Recently, the world was engulfed by a pandemic induced by a novel human coronavirus 2 (severe acute respiratory syndrome coronavirus 2 (SARS-CoV-2)). The SARS-CoV-2 virus particles are roughly spherical with radii of 80−100 nm.[1,2] The exterior of the virus particles exhibits lipid-embedded, protein-based spikes of 10−20 nm,[2] which mediate the receptor binding and membrane fusion between the virus and host cell. SARS-CoV-2, in particular, showed a relatively high stability on different types of surfaces. Viable viruses were detected on plastic and stainless steel up to 72 h after virus exposure.[3] As a result, surface transmission is one of the possible ways of coronavirus transmittal.[4] Thus, innovative and effective approaches for inactivation and limitation of the spread of viruses via surfaces are paramount.

Antiviral properties are present in different types of surfaces, both of natural and artificial origin. Many plants have been demonstrated to contain antiviral compounds that can directly destroy viruses upon contact.[5] Heavy metals such as copper (Cu), gold (Au), and silver (Ag) have been used for centuries to combat the effects of viral infections (albeit, of course, only recognized as such in the last century).[6] For example, Ag nanoparticles have—by creating Ag^+ ions—been shown to possess direct antiviral properties against a wide range of viruses, in particular, human immunodeficiency virus, hepatitis B virus, herpes simplex virus, respiratory syncytial virus, and monkeypox virus.[7] Cu-based surfaces have been shown to be highly effective against different classes of viruses, including enveloped and nonenveloped, single- and double-stranded and DNA and RNA viruses.[8,9] In some of these studies, the antiviral activity of such surfaces was demonstrated against SARS, Middle East respiratory syndrome (MERS), and SARS-CoV-2.[3,10] The virucidal activity of copper, similarly to silver, relies on the release of ionic Cu species (Cu^I or/and Cu^{II}) and, in some reports, generation of oxidative oxygen species,[8,10] and these positive results prompted us to include Cu surfaces in this study.

A different metal-free approach to creating virucidal surfaces invokes the use of antiviral polymers.[11] Polymers based on polyethyleneimine (PEI)[12,13] and polyphenol ether,[14] sialic acids,[15] and carbohydrates[16] have been reported to inactivate viruses. One of the approaches in creating antiviral coatings is the immobilization of polyethylenimine (PEI) derivatives

Received: May 23, 2022
Accepted: September 23, 2022
Published: October 20, 2022

Scheme 1. (Top) General Scheme of Polymer Brush-Based Antiviral Surfaces; (Bottom) Structure of Monomers A10 and CBMA Used to Construct Quaternary Ammonium and Zwitterionic Polymer Brushes

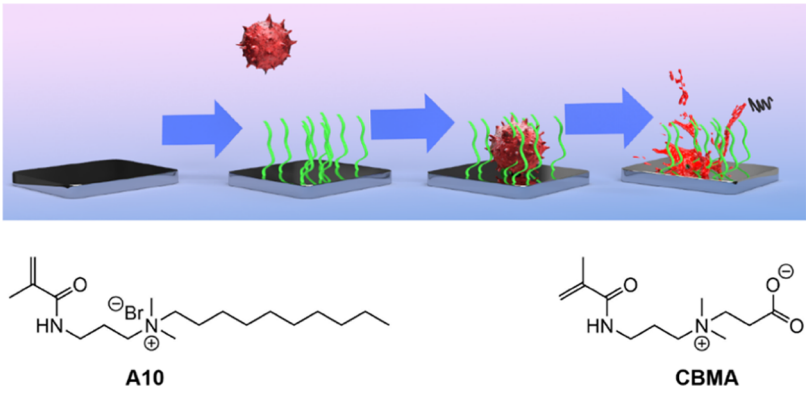

containing long-chained hydrophobic quaternary ammonium compounds on surfaces.[13,14] Upon contact, these functional groups may disrupt the virus membrane structure rendering the virus inactive. *N*,*N*-Dodecyl,methyl-polyethylenimine (DMPEI) was found to be active against both wild-type and drug-resistant strains of influenza viruses by disrupting their lipid envelopes, resulting in visibly damaged viral particles.[17,18] That lipid envelope, known as the lipid bilayer, is the "scaffold" of the virus particle onto which functional proteins are bound, and within which the RNA is protected. Thus, disruption in the structure of the lipid layer compromises the structure of the virus. Consequently, it is a viable target in the inactivation of the virus.

Polymer brushes are high-density systems that are covalently attached to surfaces.[19,20] Coatings based on polymer brushes are extensively used to create antifouling, bioactive, and antibacterial surfaces.[21−37] The high density of the polymer chains in the coating on the surfaces gives unique properties for the final layer.[19,38,39] The most commonly used method for constructing polymer brushes is surface-initiated atom transfer radical polymerization (SI-ATRP), due to the high control and possibility to initiate growth from a self-assembled monolayer.[20,26] However, SI-ATRP requires the use of heavy metals, typically copper, as catalysts. Moreover, the need for rigorous deoxygenation to achieve polymerization makes this approach difficult to scale and experimentally challenging to apply. The ease of coating was further increased, and the possibility to surface patterning was introduced using techniques such as single-electron transfer living radical polymerization (SET-LRP)[34] and light-triggered living radical polymerization (LT-LRP),[22] but those methods still used heavy-metal catalysts. Thus, controlled polymerization approaches based on thermally initiated reversible addition-fragmentation chain transfer (RAFT)[40,41] polymerization and its surface-initiated (SI-RAFT)[24] analogue were introduced, which allow polymerizations without the need for heavy metals, although they still require an oxygen-free environment.

Recently, a new RAFT-based technique was introduced: photoinduced electron transfer-reversible addition-fragmentation chain transfer (PET-RAFT).[42−45] We and others further developed this method, labeled surface-initiated PET-RAFT, or SI-PET-RAFT, into an efficient and extremely mild (visible-light-driven, oxygen-tolerant, in water) way to covalently coat surfaces and applied this to the construction of polymer brushes.[21,45−47] This polymerization technique can proceed in an aqueous solution containing a suitably chosen dye, here: eosin Y (EY), as a photocatalyst and allows for the visible-light-induced patterned growth of complex polymer brushes in a controlled manner in the presence of oxygen in the water. A mechanism and the living nature of PET-RAFT polymerizations were previously postulated by Xu et al.[48] They proposed that the reaction proceeds according to a reductive quenching cycle of eosin Y in which triethanolamine acts as a sacrificial electron donor to reduce oxygen in the polymerization system. The reduction of oxygen allows the polymerization to proceed in an oxygen-containing environment, which is the main advantage of this technique in contrast to SI-ATRP and SI-RAFT. We, therefore, envisioned SI-PET-RAFT to be a potentially viable route for the construction of quaternary ammonium-based antiviral coatings.

Finally, since surface roughness has also been reported as a likely factor in antiviral activity,[11] while we aimed to study the specific effects of the chemical functionalities involved, only smooth surfaces (i.e., nonstructured and atomic force microscopy (AFM)-measured roughness ≤3.5 nm) were used.

This paper investigates the antiviral properties of copper surfaces and polymer brushes containing quaternary ammonium moieties as constructed with the SI-PET-RAFT technique. A new methacrylic derivative of *N*,*N*-dodecyl,methyl-polyethylenimine, *N*-[3-decyldimethyl-aminopropyl] methacrylamide bromide (**A10**) was synthesized for such polymer brushes. We envisioned that polymer brushes based on **A10** monomers would be able to render viruses inactive by penetrating their membranes (Scheme 1). In addition, carboxybetaine methacrylamide (**CBMA**)-based brushes previously showed antibacterial and antifouling properties.[21,49,50] To the best of our knowledge, however, no antiviral studies have been reported for these brushes, and these **A10**- and **CBMA**-coated surfaces were now tested in parallel for their antiviral properties. The chemical composition, thickness, roughness, and wettability of the resulting polymer brush coatings were characterized extensively by X-ray photoelectron spectroscopy (XPS), atomic force microscopy (AFM), water contact angle measurements, and ellipsometry. The antiviral properties of coatings were investigated by exposure to SARS-CoV-2 and avian influenza and measured in terms of the amount of viable virus after a specific time. The economic and humanitarian damages of the annually returning influenza virus pandemics are also well analyzed and studied,[51] yet the structure of avian flu virus is rather different from that of SARS-CoV-2, motivating why this virus type was chosen as the

https://doi.org/10.1021/acsomega.2c03214
ACS Omega 2022, 7, 38371−38379

second candidate for this model study to better display the scope of our findings.

EXPERIMENTAL SECTION

Materials. All chemical reagents were used without further purification unless otherwise specified. 4-Cyano-4-(phenylcarbonothioylthio)pentanoic acid *N*-succinimidyl ester (RAFT-NHS), *N*-[3-(dimethylamino)propyl]-methacrylamide, 1-bromodecane, (3-aminopropyl)-triethoxysilane (APTES), triethanolamine (TEOA), eosin Y (EY), triethylamine (TEA), ethanol (EtOH, 99.9%), acetone (99.5%), dry tetrahydrofuran (THF, 99.9%), dry diethyl ether (99.9%), and acetonitrile (99.9%) were purchased from Sigma-Aldrich. Carboxybetaine methacrylamide (**CBMA**) was synthesized according to a previously described procedure.[31,52,53] Silicon substrates were acquired from Siltronix. Deionized water was produced with a Milli-Q integral 3 system (Millipore, Molsheim, France (Milli-Q water)).

Synthesis of *N*-[3-(Alkyldimethyl)-aminopropyl]-methacrylamide Bromide Monomer (A10). Monomer **A10** was synthesized via a quaternization reaction of *N*-[3-(dimethylamino)propyl]methacrylamide and 1-bromodecane, according to a slight modification of a previously reported procedure.[54] In a round-bottom flask with a septum, 10 mL of acetonitrile was added to a mixture of *N*-[3-(dimethylamino)-propyl]methacrylamide (0.03 mol, 5.10 g, 4.79 mL), 1-bromodecane (0.03 mol, 6.64 g), and a small amount of an inhibitor (hydroquinone). The flask was sealed with a septum under argon and heated at 50 °C under magnetic stirring for 24 h. Upon addition of 250 mL of dry ethyl ether to the reaction mixture, *N*-[3-(decyldimethyl)-aminopropyl]-methacrylamide bromide (**A10**) was isolated as white crystals and dried (7.00 g, yield 60%). The monomer was characterized by ^{1}H NMR and electrospray ionization (ESI).

N-[3-(Decyldimethyl)-aminopropyl]methacrylamide bromide (**A10**) (Figure S1): ^{1}H NMR (dimethyl sulfoxide (DMSO), 400 MHz, δ in ppm): 0.86 (t, 3H, CH_3 (22)), 1.26 (m, 14H, CH_2 (15, 16, 17, 18, 19, 20, 21)), 1.62 (m, 2H, CH_2 (14)), 1.87 (m, 5H, CH_2 (6, 9)), 3.01 (s, 6H, N^+-CH_3 (11, 12)), 3.25 (m, 6H, CH_2 (5, 7, 13)), 5.35 (s, 1H, HC=CCH_3 CH_2(1″)), 5.70 (s, 1H, HC=C(1′)), 8.10 (t, 1H, NH) (Figure S1). Mass ESI: measured: 311.3048. theoretical (M^+): 311.3062.

Mass Spectrometry (MS). MS data were recorded on an Exactive high-resolution MS instrument (Thermo Scientific) equipped with an electrospray ionization (ESI) probe. The MS was calibrated daily using ProteoMass LTQ/FT-hybrid ESI Pos. Mode Cal. Mix and Pierce ESI Neg. Ion Cal. solutions. Thermo Xcalibur Browser software version 2.2 was used for instrument control, data acquisition, and data processing. The ESI mass spectra were obtained over the range of m/z 100–750. The exact mass of compound **A10** was determined with a precision of 3 ppm.

Light Source. Light-emitting diodes (LEDs) with a maximum intensity at 410 nm (Intelligent LED Solutions product number: ILH-XO01-S410-SC211-WIR200) were used. The input current was set at 700 mA, corresponding to a total radiometric power of 2.9 W, according to manufacturer specifications.

Formation of RAFT Agent-Functionalized Monolayers. The monolayers were created according to previously published procedures.[21,47]

SI-PET-RAFT Synthesis of Polymer Brushes. The poly(**CBMA**) brushes were synthesized by a previously published technique.[21,47] The poly(**A10**) brushes were prepared according to a previously reported protocol with slight modifications.[21,47] A stock solution with photocatalyst was prepared to contain EY (25 mg, 39 μmol) and TEOA (160 mg, 1.6 mmol) in 10 mL of Milli-Q water. The monomer **A10** (0.31 mmol, 122 mg) was dissolved in Milli-Q water (1 mL), and subsequently, 10 μL of the stock solution was added. The mixture was vortexed and added to the vials containing surfaces with an immobilized RAFT agent. Immediately after this, the polymerization was conducted by irradiating the vials with visible light from the LED light source for controlled periods of time. The thickness of the polymerization solution on top of the surfaces was 2 mm. In these experiments, the light source was placed 3–4 cm from the substrates, to prevent substantial heating of the samples with the light. Afterward, a copious amount of EtOH was added to the samples to remove unbound polymers from the surface, and further cleaning was obtained by subsequent rinsing with EtOH and Milli-Q water. Finally, the coated samples were blown dry under a stream of Ar.

In addition, the reaction was conducted on a complete 100 mm silicon wafer to provide the necessary amount of surfaces for the antiviral tests. The polymerization solution was scaled up from 1 to 30 mL, and for this purpose, a custom-made reactor 200 × 200 × 2.0 mm^3 was designed and used (see setup in Figure S2).

X-ray Photoelectron Spectroscopy (XPS). XPS measurements were performed using a JPS-9200 photoelectron spectrometer (JEOL Ltd., Japan). All of the samples were prepared and stored under ambient conditions prior to analysis using a focused monochromated Al Kα X-ray source (spot size of 300 μm) radiation at 12 kV and 20 mA, with 10 eV as analyzer pass energy. XPS wide-scan and narrow-scan spectra were obtained under ultrahigh-vacuum (UHV) conditions (base pressure 3 × 10^{-7} Pa). All narrow-range spectra were corrected with a linear background before fitting. The spectra were fitted with symmetrical Gaussian/Lorentzian (GL(30)) line shapes using CasaXPS. All spectra were referenced to the C 1s peak attributed to C–C and C–H atoms at 285.0 eV.[55]

Static Water Contact Angle (SWCA) Measurements. The wettability of the modified surfaces was determined by automated static water contact angle measurements with the use of a Kruss DSA 100 goniometer. The volume of a drop of demineralized water was 3 μL. Contact angles from sessile drops measured by the tangent method were estimated using a standard error propagation technique involving partial derivatives.

Spectroscopic Ellipsometry. Polymerization kinetics were followed by measuring the dry thickness of the brushes using an Accurion Nanofilm_ep4 Imaging Ellipsometer. The ellipsometric data were acquired in air at room temperature (RT) using light in the wavelength range of λ = 400.6–761.3 nm at an angle of incidence of 50°. The data were fitted with EP4 software using a multilayer model. The model consisted of a silicon (Si) bottom layer covered with a thin SiO_2 layer of 0.3 nm. Then, the polymer brush layers were described using a Cauchy model with parameters A = 1.526 and B = 1221 for poly(**CBMA**) and A = 1.540 and B = 334 for poly(**A10**).

Atomic Force Microscopy (AFM). AFM surface topography images were acquired by an Asylum Research MFP-3D Origin AFM (Oxford Instruments, U.K.). The instrument

https://doi.org/10.1021/acsomega.2c03214
ACS Omega 2022, 7, 38371–38379

Scheme 2. General Scheme for the Synthesis of Antiviral Polymer Brushes

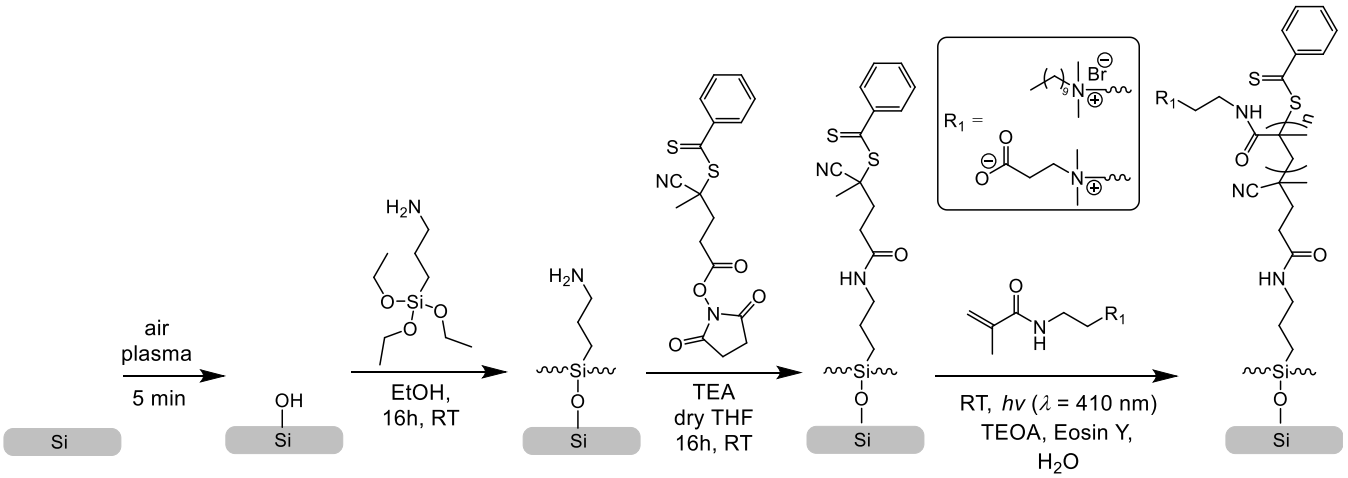

was operated in tapping mode and equipped with a silicon cantilever (AC240TS-R3, k = 1.3 N·m^{-1}) with a nominal tip radius of ∼7 nm. Gwyddion[56] and Mountains 8 (Digital Surf, France) software was used to process and analyze the AFM topography images.

Antiviral Activity. The following low pathogenic avian influenza strain was used: H5N2 A/Swan/Neth/11016034/11. To culture avian influenza and access the amount of viable virus, Madin−Darby Canine Kidney (MDCK) cells were maintained in complete medium: Dulbecco's modified Eagle's medium, high glucose, GlutaMAX, pyruvate + 5.0% fetal bovine serum (FBS) + 0.01% penicillin−streptomycin (10,000 U·mL^{-1}; to prevent bacterial and fungal contamination). When MDCK cells were inoculated with avian influenza, the complete medium was substituted with Dulbecco's modified Eagle's medium, high glucose, GlutaMAX, pyruvate + 1.5% albumin, bovine, reagent grade + 0.5 μg·mL^{-1} trypsin from bovine pancreas.

To evaluate the antiviral properties of the polymer brushes against avian influenza, 50 μL of virus stock (dilution 1:1000) was dispersed onto the coated antiviral surfaces. After incubation periods at room temperature (RT) of 1.5, 3, 7, 24, and 72 h, possible viable virus was washed off using 500 μL of complete medium. For each time point, at least three separate surfaces were used. For the determination of viral titers, eight 10-fold serial dilutions were used to inoculate MDCK cells (described in Bergervoet et al.[57]) with the addition of 0.5 μg trypsin·mL^{-1}. After incubation at 37 °C for 4 days, plates were stained with an immunoperoxidase monolayer assay and scored for positive (stained) wells[57] with the substitution of paraformaldehyde by 4% formaldehyde. Titers were calculated using the Spearman−Kärber algorithm and were expressed as $TCID_{50}$·mL^{-1}.[58,59]

SARS-CoV-2. The SARS-CoV-2 strain used was described by Gerhards et al.[60] Vero-E6 cells were maintained in complete medium: minimum essential medium, no glutamine + 5% fetal bovine serum (FBS, qualified, Australia) + 1% L-glutamine (200 mM) + 1% minimum essential medium non-essential amino acids solution (100×) + 1% antibiotic−antimycotic solution (penicillin and streptomycin, to prevent bacterial and fungal contamination).

To access the antiviral properties of the polymer brushes against SARS-CoV-2, 50 μL of virus stock (undiluted) was dispersed onto the coated antiviral surfaces. After incubation periods at RT of 1.5, 3, 7, 24, and 72 h, a possible viable virus was washed off using 500 μL of complete medium. For each time point, at least three separate surfaces were used. For the determination of viral titers, six 5-fold serial dilutions were used to inoculate Vero-E6 cells.[60] After incubation at 37 °C for 4 days, plates were stained with an immunoperoxidase monolayer assay and scored for positive (stained) wells.[60] Titers were calculated using the Spearman−Kärber algorithm and were expressed as $TCID_{50}$·mL^{-1}.[58,59] All SARS-CoV-2 experiments were performed at the BSL3 facilities in Lelystad.

RESULTS AND DISCUSSION

The two monomers selected for the creation of potential polymer brush-based antiviral coatings were *N*-[3-decyldimethyl-aminopropyl]methacrylamide bromide (**A10**) and carboxybetaine methacrylate (**CBMA**). The **A10** monomer was synthesized via the quaternization reaction of *N*-[3-(dimethylamino)propyl]methacrylamide and 1-bromodecane according to a slight modification of a previously reported procedure (see the Experimental Section for details).[54] The antiviral polymer brush-based coatings were created in four steps starting from bare silicon surfaces according to a modified previously published protocol (Scheme 2).[21,47] The silicon surfaces were plasma cleaned for 5 min, and subsequently, (3-aminopropyl)triethoxysilane (APTES) was immobilized. The RAFT-agent monolayer was prepared by reacting the (3-aminopropyl)triethoxysilane (APTES) monolayer, immobilized on the oxidized silicon surface, with 4-cyano-4-(phenylcarbonothioylthio)pentanoic acid *N*-succinimidyl ester (RAFT-NHS). In this process, 29 ± 4% of the surface-bound amine sites react to hold a RAFT agent moiety.[21] The polymer brushes were then grown employing SI-PET-RAFT in the presence of the corresponding monomer (**A10** or **CBMA**), EY, and TEOA.

Synthesis of Antiviral Polymer Brush-Based Coatings. The thickness of brushes was determined by spectroscopic ellipsometry. The poly(**A10**) brush-based coatings achieved a thickness of 71 ± 2 nm after 1 h of polymerization, while the poly(**CBMA**) brush-based coating grew to 46 ± 4 nm after 5 h of polymerization. The AFM topography images of brush-coated surfaces showed homogeneous layers with a roughness of R_q = 3.50 ± 0.55 and 2.03 ± 0.49 nm for poly(**A10**) and poly(**CBMA**), respectively (Figures 1d,e and S5). The static water contact angle (SWCA) of coatings for poly(**A10**) was

https://doi.org/10.1021/acsomega.2c03214
ACS Omega 2022, 7, 38371−38379

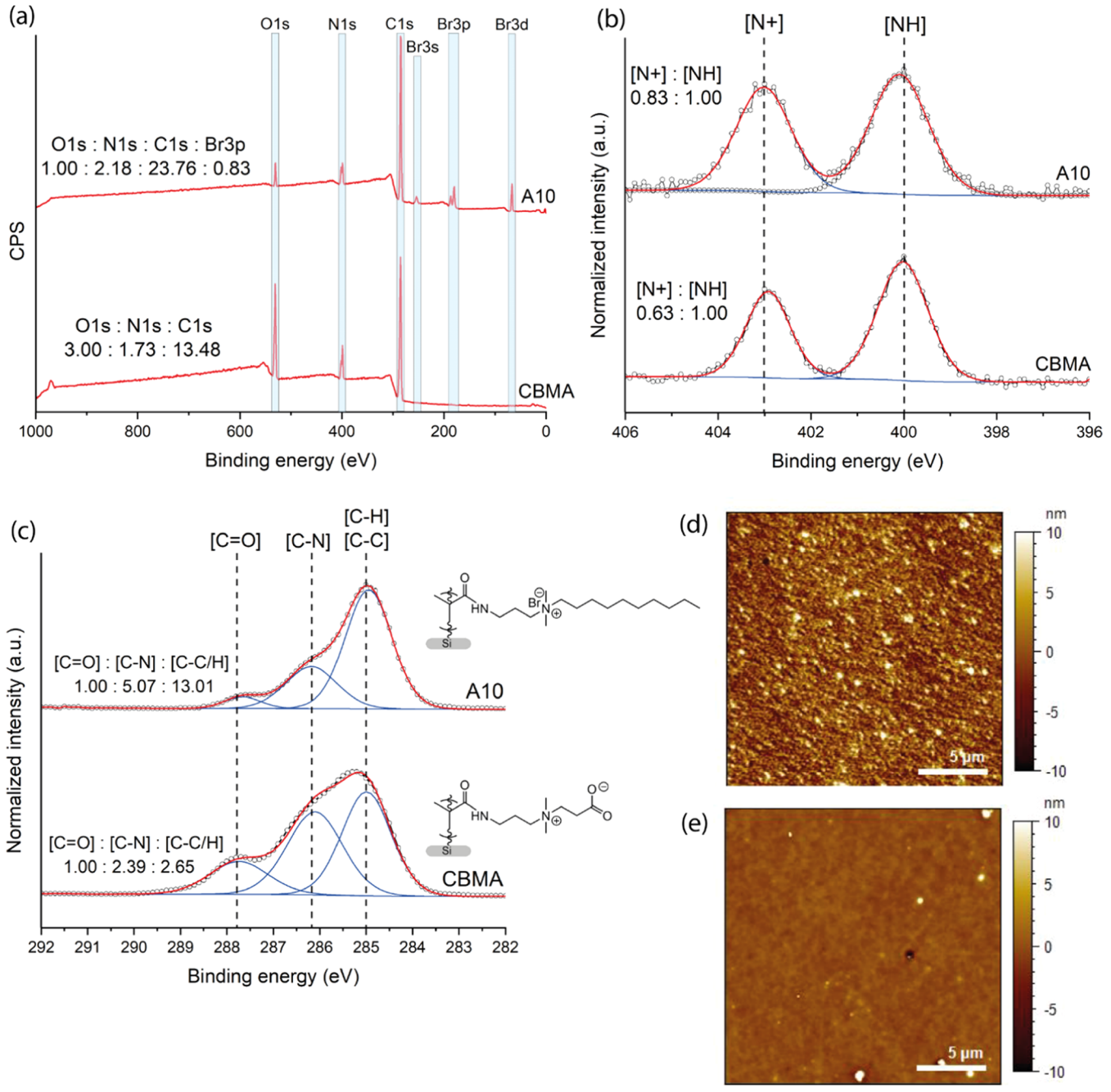

Figure 1. Physicochemical properties of polymer brush-coated surfaces. XPS wide spectra of poly(**CBMA**)- and poly(**A10**)-coated surfaces (a). XPS N 1s narrow scan (b) and XPS C 1s narrow scan (c) of poly(**CBMA**)- and poly(**A10**)-coated surfaces. Typical AFM topography images of poly(**A10**)- (d) and poly(**CBMA**)-coated surfaces (e).

determined to be 88 ± 4° and for poly(**CBMA**) 37 ± 2°. The relatively higher SWCA of poly(**CBMA**) brushes compared to polymer brushes obtained by ATRP[36] may be related not only to the high molecular weight of the resulting polymer but also to other factors like polymer confirmation, surface tension, and surface roughness.[61] In addition, the SWCA values are well aligned with previously reported values for **CBMA** obtained by nitroxide-mediated free radical polymerization-based coatings.[62] The chemical composition of the resulting polymer brushes was confirmed by XPS (Figure 1a). The wide spectra of poly(**CBMA**) brushes showed three main peaks for O 1s (531 eV), C 1s (285 eV), and N 1s (400 eV) in a ratio of 3.0:13.5:1.7, in reasonable agreement with the theoretical ratio of poly(**CBMA**) brushes, 3:12:2. The poly(**A10**) brushes were characterized using XPS as well, and the wide spectra showed four main peaks, for O 1s (531 eV), C 1s (285 eV), N 1s (400 eV), and Br 3s (255 eV) (secondary peaks: Br 3p (181 eV) and Br 3d (69 eV)) in a ratio of 1.0:23.8:2.2:0.8, while the theoretical ratio was 1:19:2:1. The relatively higher amount of carbon in both polymer brush structures is attributed to atmospheric contamination.

The XPS C 1s narrow-scan spectrum for poly(**A10**) shows three main peaks, which we assign as [C−C/H] (285.0 eV)/[C−N] (286.2 eV)/[HN−C═O] (287.8 eV) moieties in a ratio of 13.0:5.1:1.0 (theoretical ratio is: 13:5:1), and for poly(**CBMA**), these peaks appear in a ratio of 2.7:2.4:1.0

https://doi.org/10.1021/acsomega.2c03214
ACS Omega 2022, 7, 38371−38379

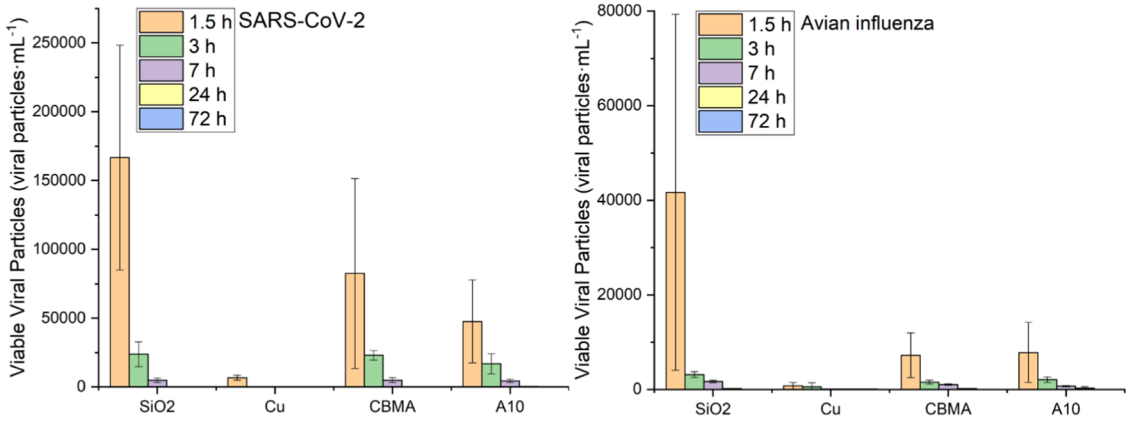

Figure 2. Antiviral activity of copper-coated surfaces, and poly(**CBMA**) and poly(**A10**) brush surfaces against SARS-CoV-2 and avian influenza. Plasma-cleaned silicon surfaces were used as a negative control.

(theoretical ratio: 2.5:2.5:1.0) (Figure 1c). The narrow XPS spectra for the poly(**A10**) brushes were simulated applying core orbital energy levels as obtained by density functional theory (DFT),[63,64] and the simulated spectra (Figure S3) agreed well with experimental data, supporting our assignment. The narrow N 1s spectra of poly(**CBMA**) and poly(**A10**) brushes show two peaks that correspond to [N^+] (403 eV) and [NH] (400 eV) in ratios of 0.63:1.00 and 0.83:1.00, respectively (Figure 1b). The relatively lower than theoretically expected value [for both monomers 1:1] can be related to the degradation of [N^+] moieties under heat, in vacuo conditions, and exposure to X-ray beams during the XPS measurement, as noted for poly(**CBMA**) coatings by van Andel et al.[50]

Copper-Coated Surfaces. A custom-produced silicon wafer was used that was homogeneously coated with a copper layer (thickness Cu layer = 200 nm; AFM-determined roughness R_q = 1.74 ± 0.11 nm, SWCA 94 ± 3°; see Figure S4).

Control Surfaces. Neutral unmodified plasma-cleaned silicon surfaces, with a measured roughness of R_q = 0.68 ± 0.10 nm, were used as a negative control (Figure S4b). The wide-scan XPS spectra of these silicon surfaces showed the predominance of silicon oxide (Figure S4a).

Antiviral Studies. We exposed our surfaces to SARS-CoV-2 and avian influenza. In a typical experiment, a 50 μL drop of virus stock containing SARS-CoV-2 and avian influenza was deposited on the different types of surfaces. These solutions contained for SARS-CoV-2 ca. 69,000 viable viral particles·mL^{-1} and for avian influenza ca. 54,800 viable viral particles·mL^{-1}. The drop was left on the surface for different periods of time, ranging from 1.5 to 72 h (Figure 2 and Tables S1 and S2). Subsequently, surfaces were washed, and the exact number of viable viral particles was determined by $TCID_{50}$·mL^{-1} titration (see the Experimental Section for details).

First, the copper-coated surfaces showed the best antiviral activity toward both SARS-CoV-2 and avian influenza. Compared to our negative control (SiO_2), copper inactivates SARS-CoV-2 at least 20 times faster, while for avian influenza, the number after 1.5 h is about 50 times smaller than on silicon oxide. These results indicate that, in cases where the toxicity of copper ions does not play a significant role, infusion of copper might be a viable manner to turn a surface antiviral. This high activity of copper is in line with related studies of SARS-CoV-2 and other viruses.[3,8−10] Likely, part of the virus-killing mechanism also affects cells, making copper both a good antiviral agent and toxic for humans. Therefore, metal-free solutions are also badly needed.

Second, the amount of SARS-CoV-2 viable virus on the poly(**CBMA**) and poly(**A10**) after 1.5 h of incubation was two to three times lower compared to the bare silicon surface. The polymer brush coatings incubated with avian influenza virus decreased the amount of viable virus in comparison to bare silicon surfaces even up to 5−6 times. After 3 h of incubation of viable SARS-CoV-2 and avian influenza virus on poly(**CBMA**) and poly(**A10**) surfaces decreased 4−5 times and 3−4 times correspondingly in relation to the amount of virus detected after 1.5 h of incubation. Furthermore, brush-based coatings inactivated most of the deposited virus on the surfaces within 7 h of incubation. Although difficult to compare quantitatively, this compares positively to SAR-CoV-2 surviving even up to 72 h on steel and plastic,[3] and these findings might imply that our "negative control" displays some antiviral activity as well. The poly(**CBMA**) and poly(**A10**) brushes thus overall show comparable antiviral activity toward SARS-CoV-2 and avian influenza. While not as effective as copper, the poly(**CBMA**) and poly(**A10**) coatings do not contain heavy metals. Moreover, poly(**CBMA**)-based coatings and polymers previously demonstrated good antifouling and biocompatible properties.[49,50,65] A probable antiviral mechanism for poly(**A10**) brushes, as previously reported for DMPEI compounds mechanics,[17,18] is based on penetration of the virus membrane and rendering it inactive (Scheme 3). Such a route would likely not apply for poly(**CBMA**), which does not have large aliphatic tails in its structure, yet shows a comparable antiviral activity. Previously, zwitterionic and cationic PEI derivatives (*N*-(15-carboxypentadecyl)-PEI HCl salt) containing long aliphatic chains in the comparable study showed similar antiviral activity.[13] It should be noted that **CBMA** is overall a much smaller moiety with more closely spaced charge positions and significantly higher hydrophilicity than previously investigated PEI zwitterionic derivatives. Thus, the pathway toward virus dismantling may be also related to the presence of quaternary ammonium cation in poly(**CBMA**) and poly(**A10**) brushes. The mechanism of antiviral activity of both brush coatings can also be absolutely different. While the positive charge and hydrophobic part play a key role in dismantling the virus for **A10** brushes, the strong affinity to water and previously reported antifouling properties of the **CBMA** brush might explain the antiviral activity of those brushes. It should be noted that at this stage, the mechanism of

https://doi.org/10.1021/acsomega.2c03214
ACS Omega 2022, 7, 38371−38379

Scheme 3. General Scheme of the Suggested Antiviral Mechanism of Lipid Bilayer-Disrupting Polymer Brushes (1−3); Monomer Chemical Structure and Monomer Schematic Representation Are Shown Below

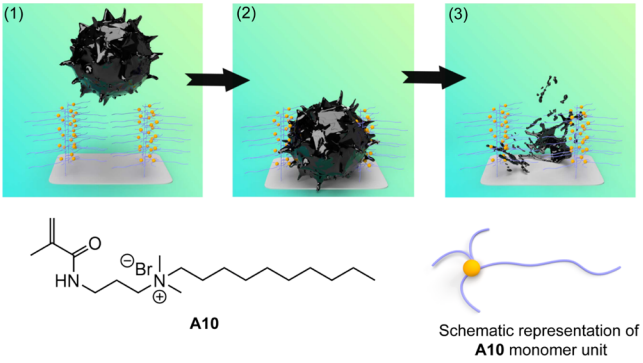

antiviral activity of the brushes is unknown and may be related to many factors including the combination superstructure of the brush itself and positively charged moieties along the chain.

The effect of the porosity on the micron scale was previously reported as an important factor in virus survival on the surface.[66] In our study, both the synthesized surfaces and control surfaces are all basically flat (AFM topography displays roughnesses only in the range of a few nanometers; see Figures 1d,e and S3). As a result, differences in porosity or roughness likely play no significant role in determining the differences observed in our measurements.

Finally, the facile way to apply SI-PET-RAFT for creating polymer brush coatings, requiring only visible light to supply the driving force, might open up a range of applications where alternatives—from ventilating rooms to frequent cleaning—do not suffice. One can, for example, envision such coatings on common frequent-contact surfaces, such as plastic cards, touch screens, door handles, and walls. Here, the minimal toxicity of bioinert polymer brushes, in particular, poly(**CBMA**) brushes, would allow application in areas that would be unthinkable for toxic coatings such as copper. Eventually, such applications could also be applied to plastics such as PPE or rubbery materials to help diminish the risk of sexually transmitted infections or those transmittable by touch. Finally, it is likely that the combination of chemical and physical effects together (chemically well-chosen functional groups on a surface with optimal micro/nanostructuring, for example) will be needed for optimal results. Such work is currently ongoing in our laboratories.

CONCLUSIONS

A new route was developed for creating antiviral coatings based on copper coating and on polymer brushes synthesized by surface-initiated photoinduced electron transfer-reversible addition-fragmentation chain transfer (SI-PET-RAFT). Copper-coated surfaces are very effective, speeding up the inactivation of the virus about 25−50 times compared to a silicon oxide negative control. Both quaternary ammonium polymer brushes and zwitterionic polymer brushes strongly, and more or less equally, sped up the process of inactivating viruses, with a reduction of factor 5−6 times for avian flu and a factor 2−3 times for SARS-CoV-2. In both cases, nearly all virus activity reached down to detection levels after about 7 h. Since SI-PET-RAFT is scalable, oxygen-tolerant, driven by visible light, can take place in water, and is applicable to almost any surface, we envision the significant potential of our approach in the further study and development of antiviral surfaces, likely in combination with the optimization of surface structuring.

ASSOCIATED CONTENT

Supporting Information

The Supporting Information is available free of charge at https://pubs.acs.org/doi/10.1021/acsomega.2c03214.

^{1}H NMR spectrum of *N*-[3-(decyldimethyl)-aminopropyl]methacrylamide bromide (**A10**); scale-up photoreactor scheme; simulated C 1s XPS spectra; wide-scan XPS spectra of the silicon and copper surfaces used in antiviral tests and AFM topography; viable viral particles of SARS-CoV-2 on different surfaces at different periods of time; viable viral particles of avian influenza on different surfaces at different periods of time (PDF)

AUTHOR INFORMATION

Corresponding Author

Han Zuilhof − *Laboratory of Organic Chemistry, Wageningen University, 6708 WE Wageningen, The Netherlands; School of Pharmaceutical Sciences and Technology, Tianjin University, Tianjin 300072, People's Republic of China; Department of Chemical and Materials Engineering, Faculty of Engineering, King Abdulaziz University, 21589 Jeddah, Saudi Arabia;* orcid.org/0000-0001-5773-8506; Email: han.zuilhof@wur.nl

Authors

Andriy R. Kuzmyn − *Laboratory of Organic Chemistry, Wageningen University, 6708 WE Wageningen, The Netherlands;* orcid.org/0000-0002-1571-2911

Lucas W. Teunissen − *Laboratory of Organic Chemistry, Wageningen University, 6708 WE Wageningen, The Netherlands;* orcid.org/0000-0003-0018-1211

Michiel V. Kroese − *Wageningen Bioveterinary Research, 8221 RA Lelystad, The Netherlands*

Jet Kant − *Wageningen Bioveterinary Research, 8221 RA Lelystad, The Netherlands*

Sandra Venema − *Wageningen Bioveterinary Research, 8221 RA Lelystad, The Netherlands*

Complete contact information is available at: https://pubs.acs.org/10.1021/acsomega.2c03214

Author Contributions

The manuscript was written through contributions of all authors. All authors have given approval to the final version of the manuscript.

Funding

This research was carried out under project number T20001 in the framework of the Research Program of the Materials innovation institute (M2i) (www.m2i.nl) supported by the Dutch government.

Notes

The authors declare no competing financial interest.

ACKNOWLEDGMENTS

Dr. Maarten M. J. Smulders is acknowledged for insightful discussions.

REFERENCES

(1) Bar-On, Y. M.; Flamholz, A.; Phillips, R.; Milo, R. SARS-CoV-2 (COVID-19) by the numbers. *eLife* **2020**, *9*, No. e57309.
(2) Prasad, S.; Potdar, V.; Cherian, S.; Abraham, P.; Basu, A. ICMR-NIV NIC Team, Transmission electron microscopy imaging of SARS-CoV-2. *Indian J. Med. Res.* **2020**, *151*, 241−243.
(3) van Doremalen, N.; Bushmaker, T.; Morris, D. H.; Holbrook, M. G.; Gamble, A.; Williamson, B. N.; Tamin, A.; Harcourt, J. L.; Thornburg, N. J.; Gerber, S. I.; Lloyd-Smith, J. O.; de Wit, E.; Munster, V. J. Aerosol and Surface Stability of SARS-CoV-2 as Compared with SARS-CoV-1. *N. Engl. J. Med.* **2020**, *382*, 1564−1567.
(4) Kampf, G.; Todt, D.; Pfaender, S.; Steinmann, E. Persistence of Coronaviruses on Inanimate Surfaces and Their Inactivation with Biocidal Agents. *J. Hosp. Infect.* **2020**, *104*, 246−251.
(5) Xian, Y.; Zhang, J.; Bian, Z.; Zhou, H.; Zhang, Z.; Lin, Z.; Xu, H. Bioactive Natural Compounds Against Human Coronaviruses: a Review and Perspective. *Acta Pharm. Sin. B* **2020**, *10*, 1163−1174.
(6) Davies, R. L.; Etris, S. F. The Development and Functions of Silver in Water Purification and Disease Control. *Catal. Today* **1997**, *36*, 107−114.
(7) Galdiero, S.; Falanga, A.; Vitiello, M.; Cantisani, M.; Marra, V.; Galdiero, M. Silver Nanoparticles as Potential Antiviral Agents. *Molecules* **2011**, *16*, 8894−8918.
(8) Warnes, S. L.; Summersgill Emma, N.; Keevil, C. W. Inactivation of Murine Norovirus on a Range of Copper Alloy Surfaces Is Accompanied by Loss of Capsid Integrity. *Appl. Environ. Microbiol.* **2015**, *81*, 1085−1091.
(9) Sagripanti, J. L.; Routson, L. B.; Lytle, C. D. Virus Inactivation by Copper or Iron Ions Alone and in the Presence of Peroxide. *Appl. Environ. Microbiol.* **1993**, *59*, 4374−4376.
(10) Warnes, S. L.; Little, Z. R.; Keevil, C. W. Human Coronavirus 229E Remains Infectious on Common Touch Surface Materials. *mBio* **2015**, *6*, No. e01697-15.
(11) Rakowska, P. D.; Tiddia, M.; Faruqui, N.; Bankier, C.; Pei, Y.; Pollard, A. J.; Zhang, J.; Gilmore, I. S. Antiviral Surfaces and Coatings and their Mechanisms of Action. *Commun. Mater.* **2021**, *2*, No. 53.
(12) Spoden, G. A.; Besold, K.; Krauter, S.; Plachter, B.; Hanik, N.; Kilbinger Andreas, F. M.; Lambert, C.; Florin, L. Polyethylenimine Is a Strong Inhibitor of Human Papillomavirus and Cytomegalovirus Infection. *Antimicrob. Agents Chemother.* **2012**, *56*, 75−82.
(13) Haldar, J.; An, D.; Álvarez de Cienfuegos, L.; Chen, J.; Klibanov, A. M. Polymeric Coatings that Inactivate both Influenza Virus and Pathogenic Bacteria. *Proc. Natl. Acad. Sci. U.S.A.* **2006**, *103*, 17667.
(14) Wang, Y.; Canady, T. D.; Zhou, Z.; Tang, Y.; Price, D. N.; Bear, D. G.; Chi, E. Y.; Schanze, K. S.; Whitten, D. G. Cationic Phenylene Ethynylene Polymers and Oligomers Exhibit Efficient Antiviral Activity. *ACS Appl. Mater. Interfaces* **2011**, *3*, 2209−2214.
(15) Tang, S.; Puryear, W. B.; Seifried, B. M.; Dong, X.; Runstadler, J. A.; Ribbeck, K.; Olsen, B. D. Antiviral Agents from Multivalent Presentation of Sialyl Oligosaccharides on Brush Polymers. *ACS Macro Lett.* **2016**, *5*, 413−418.
(16) Kumar, R.; Kratzer, D.; Cheng, K.; Prisby, J.; Sugai, J.; Giannobile, W. V.; Lahann, J. Carbohydrate-Based Polymer Brushes Prevent Viral Adsorption on Electrostatically Heterogeneous Interfaces. *Macromol. Rapid Commun.* **2019**, *40*, No. 1800530.
(17) Haldar, J.; Chen, J.; Tumpey, T. M.; Gubareva, L. V.; Klibanov, A. M. Hydrophobic Polycationic Coatings Inactivate Wild-type and Zanamivir- and/or Oseltamivir-resistant Human and Avian Influenza Viruses. *Biotechnol. Lett.* **2008**, *30*, 475−479.
(18) Haldar, J.; Weight, A. K.; Klibanov, A. M. Preparation, Application and Testing of Permanent Antibacterial and Antiviral Coatings. *Nat. Protoc.* **2007**, *2*, 2412−2417.
(19) Michalek, L.; Barner, L.; Barner-Kowollik, C. Polymer on Top: Current Limits and Future Perspectives of Quantitatively Evaluating Surface Grafting. *Adv. Mater.* **2018**, *30*, No. 1706321.
(20) Zoppe, J. O.; Ataman, N. C.; Mocny, P.; Wang, J.; Moraes, J.; Klok, H.-A. Surface-Initiated Controlled Radical Polymerization: State-of-the-Art, Opportunities, and Challenges in Surface and Interface Engineering with Polymer Brushes. *Chem. Rev.* **2017**, *117*, 1105−1318.
(21) Kuzmyn, A. R.; Nguyen, A. T.; Teunissen, L. W.; Zuilhof, H.; Baggerman, J. Antifouling Polymer Brushes via Oxygen-Tolerant Surface-Initiated PET-RAFT. *Langmuir* **2020**, *36*, 4439−4446.
(22) Kuzmyn, A. R.; Nguyen, A. T.; Zuilhof, H.; Baggerman, J. Bioactive Antifouling Surfaces by Visible-Light-Triggered Polymerization. *Adv. Mater. Interfaces* **2019**, *6*, No. 1900351.
(23) Pop-Georgievski, O.; Rodriguez-Emmenegger, C.; Pereira, A. d. l. S.; Proks, V.; Brynda, E.; Rypáček, F. Biomimetic Non-fouling Surfaces: Extending the Concepts. *J. Mater. Chem. B* **2013**, *1*, 2859−2867.
(24) Zamfir, M.; Rodriguez-Emmenegger, C.; Bauer, S.; Barner, L.; Rosenhahn, A.; Barner-Kowollik, C. Controlled Growth of Protein Resistant PHEMA Brushes via S-RAFT Polymerization. *J. Mater. Chem. B* **2013**, *1*, 6027−6034.
(25) Lange, S. C.; van Andel, E.; Smulders, M. M. J.; Zuilhof, H. Efficient and Tunable Three-Dimensional Functionalization of Fully Zwitterionic Antifouling Surface Coatings. *Langmuir* **2016**, *32*, 10199−10205.
(26) Kuzmyn, A. R.; de los Santos Pereira, A.; Pop-Georgievski, O.; Bruns, M.; Brynda, E.; Rodriguez-Emmenegger, C. Exploiting End Group Functionalization for the Design of Antifouling Bioactive Brushes. *Polym. Chem.* **2014**, *5*, 4124−4131.
(27) Rodriguez Emmenegger, C.; Brynda, E.; Riedel, T.; Sedlakova, Z.; Houska, M.; Alles, A. B. Interaction of Blood Plasma with Antifouling Surfaces. *Langmuir* **2009**, *25*, 6328−6333.
(28) Williams, D. F. On the Nature of Biomaterials. *Biomaterials* **2009**, *30*, 5897−5909.
(29) Rodriguez-Emmenegger, C.; Avramenko, O. A.; Brynda, E.; Skvor, J.; Alles, A. B. Poly(HEMA) Brushes Emerging as a New Platform for Direct Detection of Food Pathogen in Milk Samples. *Biosens. Bioelectron.* **2011**, *26*, 4545−4551.
(30) Liu, H.; Wang, S. Poly(N-isopropylacrylamide)-based thermo-responsive surfaces with controllable cell adhesion. *Sci. China: Chem.* **2014**, *57*, 552−557.
(31) Rodriguez-Emmenegger, C.; Brynda, E.; Riedel, T.; Houska, M.; Šubr, V.; Alles, A. B.; Hasan, E.; Gautrot, J. E.; Huck, W. T. S. Polymer Brushes Showing Non-Fouling in Blood Plasma Challenge the Currently Accepted Design of Protein Resistant Surfaces. *Macromol. Rapid Commun.* **2011**, *32*, 952−957.
(32) Baggerman, J.; Smulders, M. M. J.; Zuilhof, H. Romantic Surfaces: A Systematic Overview of Stable, Biospecific, and Antifouling Zwitterionic Surfaces. *Langmuir* **2019**, *35*, 1072−1084.
(33) Wischerhoff, E.; Badi, N.; Lutz, J.-F.; Laschewsky, A. Smart Bioactive Surfaces. *Soft Matter* **2010**, *6*, 705−713.
(34) Vorobii, M.; de los Santos Pereira, A.; Pop-Georgievski, O.; Kostina, N. Y.; Rodriguez-Emmenegger, C.; Percec, V. Synthesis of Non-fouling poly[N-(2-hydroxypropyl)methacrylamide] Brushes by Photoinduced SET-LRP. *Polym. Chem.* **2015**, *6*, 4210−4220.
(35) Jiang, S.; Cao, Z. Ultralow-Fouling, Functionalizable, and Hydrolyzable Zwitterionic Materials and Their Derivatives for Biological Applications. *Adv. Mater.* **2010**, *22*, 920−932.
(36) Pereira, A. d. l. S.; Rodriguez-Emmenegger, C.; Surman, F.; Riedel, T.; Alles, A. B.; Brynda, E. Use of Pooled Blood Plasmas in the Assessment of Fouling Resistance. *RSC Adv.* **2014**, *4*, 2318−2321.
(37) Teunissen, L. W.; Kuzmyn, A. R.; Ruggeri, F. S.; Smulders, M. M. J.; Zuilhof, H. Thermoresponsive, Pyrrolidone-Based Antifouling Polymer Brushes. *Adv. Mater. Interfaces* **2022**, *9*, No. 2101717.
(38) van der Weg, K. J.; Ritsema van Eck, G. C.; de Beer, S. Polymer Brush Friction in Cylindrical Geometries. *Lubricants* **2019**, *7*, No. 84.
(39) Yu, Y.; Brió Pérez, M.; Cao, C.; de Beer, S. Switching (Bio-) adhesion and Friction in Liquid by Stimulus Responsive Polymer Coatings. *Eur. Polym. J.* **2021**, *147*, No. 110298.
(40) Yeole, N. Thiocarbonylthio Compounds. *Synlett* **2010**, *2010*, 1572−1573.
(41) Moad, G.; Rizzardo, E.; Thang, S. H. Radical addition−fragmentation chemistry in polymer synthesis. *Polymer* **2008**, *49*, 1079−1131.

https://doi.org/10.1021/acsomega.2c03214
ACS Omega 2022, 7, 38371−38379

(42) Niu, J.; Page, Z. A.; Dolinski, N. D.; Anastasaki, A.; Hsueh, A. T.; Soh, H. T.; Hawker, C. J. Rapid Visible Light-Mediated Controlled Aqueous Polymerization with In Situ Monitoring. *ACS Macro Lett.* **2017**, *6*, 1109−1113.
(43) Lueckerath, T.; Strauch, T.; Koynov, K.; Barner-Kowollik, C.; Ng, D. Y. W.; Weil, T. DNA−Polymer Conjugates by Photoinduced RAFT Polymerization. *Biomacromolecules* **2019**, *20*, 212−221.
(44) Niu, J.; Lunn, D. J.; Pusuluri, A.; Yoo, J. I.; O'Malley, M. A.; Mitragotri, S.; Soh, H. T.; Hawker, C. J. Engineering Live Cell Surfaces with Functional Polymers via Cytocompatible Controlled Radical Polymerization. *Nat. Chem.* **2017**, *9*, 537−545.
(45) Li, M.; Fromel, M.; Ranaweera, D.; Rocha, S.; Boyer, C.; Pester, C. W. SI-PET-RAFT: Surface-Initiated Photoinduced Electron Transfer-Reversible Addition−Fragmentation Chain Transfer Polymerization. *ACS Macro Lett.* **2019**, *8*, 374−380.
(46) Kuzmyn, A. R.; Teunissen, L. W.; Fritz, P.; van Lagen, B.; Smulders, M. M. J.; Zuilhof, H. Diblock and Random Antifouling Bioactive Polymer Brushes on Gold Surfaces by Visible-Light-Induced Polymerization (SI-PET-RAFT) in Water. *Adv. Mater. Interfaces* **2022**, *9*, No. 2101784.
(47) Roeven, E.; Kuzmyn, A. R.; Scheres, L.; Baggerman, J.; Smulders, M. M. J.; Zuilhof, H. PLL−Poly(HPMA) Bottlebrush-Based Antifouling Coatings: Three Grafting Routes. *Langmuir* **2020**, *36*, 10187−10199.
(48) Xu, J.; Shanmugam, S.; Duong, H. T.; Boyer, C. Organophotocatalysts for Photoinduced Electron Transfer-reversible Addition−fragmentation Chain Transfer (PET-RAFT) Polymerization. *Polym. Chem.* **2015**, *6*, 5615−5624.
(49) Cheng, G.; Li, G.; Xue, H.; Chen, S.; Bryers, J. D.; Jiang, S. Zwitterionic Carboxybetaine Polymer Surfaces and their Resistance to Long-term Biofilm Formation. *Biomaterials* **2009**, *30*, 5234−5240.
(50) van Andel, E.; Lange, S. C.; Pujari, S. P.; Tijhaar, E. J.; Smulders, M. M. J.; Savelkoul, H. F. J.; Zuilhof, H. Systematic Comparison of Zwitterionic and Non-Zwitterionic Antifouling Polymer Brushes on a Bead-Based Platform. *Langmuir* **2019**, *35*, 1181−1191.
(51) Sah, P.; Alfaro-Murillo, J. A.; Fitzpatrick, M. C.; Neuzil, K. M.; Meyers, L. A.; Singer, B. H.; Galvani, A. P. Future Epidemiological and Economic Impacts of Universal Influenza Vaccines. *Proc. Natl. Acad. Sci. U.S.A.* **2019**, *116*, 20786−20792.
(52) Vaisocherová, H.; Ševců, V.; Adam, P.; Špačková, B.; Hegnerová, K.; de los Santos Pereira, A.; Rodriguez-Emmenegger, C.; Riedel, T.; Houska, M.; Brynda, E.; Homola, J. Functionalized Ultra-low Fouling Carboxy- and Hydroxy-functional Surface Platforms: Functionalization Capacity, Biorecognition Capability and Resistance to Fouling from Undiluted Biological Media. *Biosens. Bioelectron.* **2014**, *51*, 150−157.
(53) Vaisocherová-Lísalová, H.; Surman, F.; Víšová, I.; Vala, M.; Špringer, T.; Ermini, M. L.; Šípová, H.; Šedivák, P.; Houska, M.; Riedel, T.; Pop-Georgievski, O.; Brynda, E.; Homola, J. Copolymer Brush-Based Ultralow-Fouling Biorecognition Surface Platform for Food Safety. *Anal. Chem.* **2016**, *88*, 10533−10539.
(54) Chaibi, W.; Ziane, A.; Benzehaim, Z.; Bennabi, L.; Guemra, K. Synthesis and Characterization of Cationic Poly(N-[3-Hexyldimethyl-Aminopropyl] Methacrylamide Bromide) Water-Soluble Polymer. *Mater. Sci. Appl. Chem.* **2016**, *33*, 40−44.
(55) Easton, C. D.; Kinnear, C.; McArthur, S. L.; Gengenbach, T. R. Practical Guides for x-ray Photoelectron Spectroscopy: Analysis of polymers. *J. Vac. Sci. Technol., A* **2020**, *38*, No. 023207.
(56) Nečas, D.; Klapetek, P. Gwyddion: an Open-source Software for SPM Data Analysis. *Open Phys.* **2012**, *10*, 181−188.
(57) Bergervoet, S. A.; Ho, C. K. Y.; Heutink, R.; Bossers, A.; Beerens, N. Spread of Highly Pathogenic Avian Influenza (HPAI) H5N5 Viruses in Europe in 2016−2017 Appears Related to the Timing of Reassortment Events. *Viruses* **2019**, *11*, 501−517.
(58) Kärber, G. Beitrag zur kollektiven Behandlung pharmakologischer Reihenversuche. *Naunyn-Schmiedebergs Arch. Exp. Pathol. Pharmakol.* **1931**, *162*, 480−483.
(59) Spearman, C. The method of 'right and wrong cases' ('constant stimuli') without Gauss's formulae. *Br. J. Med. Psychol.* **1908**, *2*, 227−242.
(60) Gerhards, N. M.; Cornelissen, J. B. W. J.; van Keulen, L. J. M.; Harders-Westerveen, J.; Vloet, R.; Smid, B.; Vastenhouw, S.; van Oort, S.; Hakze-van der Honing, R. W.; Gonzales, J. L.; Stockhofe-Zurwieden, N.; de Jong, R.; van der Poel, W. H. M.; Vreman, S.; Kortekaas, J.; Wichgers Schreur, P. J.; Oreshkova, N. Predictive Value of Precision-Cut Lung Slices for the Susceptibility of Three Animal Species for SARS-CoV-2 and Validation in a Refined Hamster Model. *Pathogens* **2021**, *10*, No. 824.
(61) Wolf, B. A. Solubility of Polymers. *Pure Appl. Chem.* **1985**, *57*, 323−336.
(62) Abraham, S.; Unsworth, L. D. Multi-functional Initiator and Poly(carboxybetaine methacrylamides) for Building biocompatible Surfaces Using "Nitroxide Mediated Free Radical Polymerization" Strategies. *J. Polym. Sci., Part A: Polym. Chem.* **2011**, *49*, 1051−1060.
(63) Giesbers, M.; Marcelis, A. T. M.; Zuilhof, H. Simulation of XPS C1s Spectra of Organic Monolayers by Quantum Chemical Methods. *Langmuir* **2013**, *29*, 4782−4788.
(64) Zhao, J.; Gao, F.; Pujari, S. P.; Zuilhof, H.; Teplyakov, A. V. Universal Calibration of Computationally Predicted N 1s Binding Energies for Interpretation of XPS Experimental Measurements. *Langmuir* **2017**, *33*, 10792−10799.
(65) Zhang, L.; Cao, Z.; Bai, T.; Carr, L.; Ella-Menye, J.-R.; Irvin, C.; Ratner, B. D.; Jiang, S. Zwitterionic hydrogels implanted in mice resist the foreign-body reaction. *Nat. Biotechnol.* **2013**, *31*, 553−556.
(66) Tiwari, A.; Devi, P. P.; Yogesh, C.; Minakshi, P.; Sagar, M. G. Survival of Two Avian Respiratory Viruses on Porous and Nonporous Surfaces. *Avian Dis.* **2006**, *50*, 284−287.

https://doi.org/10.1021/acsomega.2c03214
ACS Omega 2022, 7, 38371−38379